

Comment on acp-2022-26 titled "Review of "The impact of atmospheric motion on source-specific black carbon and the induced direct radiative effect over a river-valley region" by Liu et al.

Anonymous Referee #1

General comment

This manuscript describes how Black Carbon concentrations, measured over a little more than a month in winter 2018 together with other chemical species in PM_{2.5} in a Chinese city nestled at the bottom of a valley, vary with different transport regimes and motion scales (from local to regional).

Response: We sincerely thank the reviewer for the comments and suggestions, and we have extensively revised the relevant text and modified the content. Below are point-by-point responses—the modifications to the manuscript are included.

The topic of the manuscript fits within the scope of the journal. The methodology should be described more precisely to build confidence in the results.

Response: We revised the methods to provide more details, particularly for the optical source apportionment and SOM. Other methods also have been revised according to the reviewer's suggestions. In addition, we have provided information regarding the cluster analysis and minimum R squared method in the supplementary materials. The changes are shown in the revised version. The revised paragraphs now read as follows:

“2.2 Sampling and laboratory measurements

eBC and the absorption coefficients (b_{abs}) at 370, 470, 520, 590, 660, 880, and 950 nm wavelength were measured using an AE33 aethalometer (Magee Scientific, Berkeley, CA, USA) equipped with a PM_{2.5} cut-off inlet (SCC 1.829, BGI Inc. USA) that had a time resolution of 1 min. A Nafion® dryer (MD-700-24S-3; Perma Pure, Inc., Lakewood, NJ, USA) with a flow rate of 5 L min⁻¹ was used to dry the PM_{2.5} before the measurement. Briefly, the particles were dried by the Nafion® dryer before being measured with the AE33 aethalometer, and the deposited particles were irradiated by light-emitting diodes at seven wavelengths of light-emitting diodes ($\lambda = 370, 470, 520, 590, 660, 880, \text{ and } 950 \text{ nm}$), and the light attenuation was detected. The non-linear loading issue for filter-based absorption measurement was accounted for in the AE33 by a technique called dual-spot compensation. The quartz filter (PN8060) matrix scattering effect was corrected by using a factor of 1.39. More details of AE33 measurement techniques can be found in Drinovec et al. (2015).

The scattering coefficient (b_{scat}) at a single (525) nm wavelength was measured with the use of a nephelometer (Aurora-1000, Ecotech, USA) that had a time resolution of 5 min. The nephelometer and aethalometer operated simultaneously and used the same PM_{2.5} cyclone and Nafion® dryer. The calibration was conducted based on the user guide with a calibration gas R-134. Zero calibrations were conducted every other day by using clean air without particles. The ambient air was drawn in through a heated inlet with a flow rate of 5 L min⁻¹. The relative humidity remained lower than 60%.

PM_{2.5} samples were collected for every 24 hours (h) from 10 a.m. local time to the 10 a.m. the next day from 16th November 2018 to 21st December 2018 with two sets of mini-volume samplers (Airmetrics, USA), one using quartz fiber filters (QM/A; Whatman, Middlesex, UK) and the other with Teflon® filters (Pall

Corporation, USA), both with a flow rate of 5 L min⁻¹. Those samples were kept in a refrigerator at 4°C before analysis. The mass concentration of K⁺ in the PM_{2.5} quartz sample was extracted in a separate 15 mL vials containing 10 mL distilled deionized water (18.2 MΩ resistivity). The vials were placed in an ultrasonic water bath and shaken with a mechanical shaker for 1 h to extract the ions and determined by a Metrohm 940 Professional IC Vario (Metrohm AG., Herisau, Switzerland) with Metrosep C6-150/4.0 column (1.7 mmol/L nitric acid+1.7 mmol/L dipicolinic acid as the eluent) for cation analysis. A group of elements (i.e. Mg, Al, Si, S, Cl, Ca, V, Mn, Fe, Ni, Cu, As, Se, Br, Sr, Pb, Ga, and Zn) on the Teflon® filters was determined by energy-dispersive x-ray fluorescence (ED-XRF) spectrometry (Epsilon 4 ED-XRF, PANalytical B.V., Netherlands). The X-rays were generated from a gadolinium anode on a side-window X-ray tube. A spectrum of the ratio of X-ray and photon energy was obtained after 24 minutes of analysis for each sample with each energy peak characteristic of a specific element, and the peak areas were proportional to the concentrations of the elements. Quality control was conducted on a daily basis with test standard sample.

Organic carbon (OC) and elemental carbon (EC) in each sample were determined with the use of a DRI Model 2001 Thermal/Optical Carbon Analyzer (Atmoslytic Inc., Calabasas, CA, USA). The thermal/optical reflectance (TOR) method and IMPROVE_A protocol were used for analysis. A punch of a quartz filter sample was heated at specific temperatures to obtain data for four OC fractions and three EC fractions. Total OC was calculated by summing all OC fractions and the pyrolyzed carbon (OP) produced. Total EC was calculated by summing all EC fractions minus the OP. Detailed methods and quality assurance/quality control processes were described in Cao et al., (2003). Primary organic carbon (POC) was estimated by using the minimum R-squared (MRS) method, which is based on using eBC as a tracer (Text S1). The method uses the minimum R² between OC and eBC to indicate where the ratio for which secondary OC and eBC are independent. A detailed description of the MRS method can be found in Wu et al., (2016).

Data for NO_x, wind speed, and direction at 12 ground monitoring sites were downloaded from http://sthjt.shaanxi.gov.cn/hx_html/zdjkqy/index.html. The wind data at 100 meters (m) above the ground and the planetary boundary layer height were downloaded from <https://rda.ucar.edu/datasets/ds633.0>. The data used for the Hybrid Single-Particle Lagrangian Integrated Trajectory (HYSPLIT) model was downloaded from Global Data Assimilation System and it had a resolution of 1°×1° (GDAS, <https://www.ready.noaa.gov/gdas1.php>). The data and main parameters used in trajectory model are listed in Table S2.”

2.3 Optical source apportionment

The positive matrix factorization (PMF) model that was used for the optical source apportionment in this study. PMF solves chemical mass balance by decomposing the observational data into different source profiles and contribution matrices as follows:

$$X_{ij} = \sum_{k=1}^p g_{ik}f_{kj} + e_{ij} \quad (1)$$

where X_{ij} denotes the input data matrix; p is the number of sources selected in the model; g_{ik} denotes the contribution of the k^{th} factor to the i^{th} input data; f_{kj} represents the k^{th} factor's profile of the j^{th} species; and e_{ij} represents the residual. Both g_{ik} and f_{kj} are non-negative. The uncertainties of each species and $b_{\text{abs}}(\lambda)$ were calculated by the equation recommended in EPA PMF5.0 user guideline(Norris et al, 2014) as follows:

$$Unc = \sqrt{(\text{error fraction} \times \text{concentration}(\text{or lighth absorption coefficient}))^2 + (0.5 \times MDL)^2} \quad (2)$$

$$Unc = \frac{5}{6} \times MDL \quad (3)$$

where MDL is the minimum detection limit of the method. When the concentration of a species was higher than the MDL then equation (2) was used otherwise equation (3) was used. In equation (2), for calculating the uncertainty of a chemical species, the error fraction was multiplied the concentration of the species. For

calculating the uncertainty of optical data, the error fractions were multiplied by the light absorption coefficients.

Chemical species data (EC, POC, K⁺, Mg, Al, Si, S, Cl, Ca, V, Mn, Fe, Ni, Cu, As, Se, Br, Sr, Pb, Ga and Zn) and the primary absorption coefficients (Pabs) data at $\lambda=370\text{nm}, 470\text{nm}, 520\text{nm}, 660\text{nm},$ and 880nm were used for PMF analysis. The error fraction of offline measured data was the difference between multiple measurements of the same sample. The error fraction used for optical data was 10% based on Rajesh and Ramachandran (2018). PMF solves the equation (1) by minimizing the Q value, which is the sum of the normalized residuals' squares, as follows,

$$Q = \sum_{i=1}^n \sum_{j=0}^n \left[\frac{e_{ij}}{u_{ij}} \right]^2 \quad (4)$$

where u_{ij} represents the uncertainties of each X_{ij} and $Q_{\text{true}}/Q_{\text{exp}}$ was used as the indicators for the factor number determination.

2.4 eBC source apportionment

The quantities of eBC generated from biomass burning versus fossil fuel combustion were deconvolved by an aethalometer model which uses Beer-Lambert's Law to write the absorption coefficients equations, wavelengths and absorption Ångström exponents (AAEs) for the two different BC emission sources (Sandradewi et al., 2008). This approach is widely used for separating BC from two different sources based on optical data (Rajesh et al., 2018; Kant et al., 2019; Panicker et al., 2010). However, the traditional aethalometer model could be affected by the light absorbing substances at lower wavelengths such as dust and secondary formation particles. An improvement to the traditional aethalometer model was made, by explicitly considering the interference of the b_{abs} at a lower wavelength (370nm) caused by dust and secondary OC. Thus, the calculation of the absorption and source apportionment was based on the following equations (Wang et al., 2020):

$$\frac{b_{\text{abs}}(370)_{\text{fossil}}}{b_{\text{abs}}(880)_{\text{fossil}}} = \left(\frac{370}{880} \right)^{-AAE_{\text{fossil}}} \quad (5)$$

$$\frac{b_{\text{abs}}(370)_{\text{biomass}}}{b_{\text{abs}}(880)_{\text{biomass}}} = \left(\frac{370}{880} \right)^{-AAE_{\text{biomass}}} \quad (6)$$

$$b_{\text{abs}}(880) = b_{\text{abs}}(880)_{\text{fossil}} + b_{\text{abs}}(880)_{\text{biomass}} \quad (7)$$

$$b_{\text{abs}}(370) = b_{\text{abs}}(370)_{\text{fossil}} + b_{\text{abs}}(370)_{\text{biomass}} + b_{\text{abs}}(370)_{\text{secondary}} + b_{\text{abs}}(370)_{\text{dust}} \quad (8)$$

$$eBC_{\text{fossil}} = \frac{b_{\text{abs}}(880)_{\text{fossil}}}{MAC_{BC}(880)_{\text{fossil}}} \quad (9)$$

$$eBC_{\text{biomass}} = \frac{b_{\text{abs}}(880)_{\text{biomass}}}{MAC_{BC}(880)_{\text{biomass}}} \quad (10)$$

where AAE_{fossil} and AAE_{biomass} are the AAEs for fossil fuel combustion and biomass burning. These were derived from the optical source apportionment by using PMF as discussed in section 3.1. Further, $b_{\text{abs}}(370)$ and $b_{\text{abs}}(880)$ are the total b_{abs} measured by the AE33 at the wavelengths of 370 nm and 880 nm respectively; $b_{\text{abs}}(370)_{\text{fossil}}$ and $b_{\text{abs}}(880)_{\text{fossil}}$ are the b_{abs} caused by emissions from fossil fuel combustion at those two wavelengths; $b_{\text{abs}}(370)_{\text{biomass}}$ and $b_{\text{abs}}(880)_{\text{biomass}}$ are the b_{abs} caused by emissions from biomass burning at those two wavelengths; $b_{\text{abs}}(370)_{\text{dust}}$ refers to the b_{abs} contributed by mineral dust at the wavelength of 370 nm, which was derived from the result of optical source apportionment; $b_{\text{abs}}(370)_{\text{secondary}}$ refers to the b_{abs} caused by the secondary aerosols at the wavelength of 370 nm, which was calculated by the minimum R -squared approach with eBC as a tracer (Text S1, Wang et al., 2019); eBC_{fossil} and eBC_{biomass} are the eBCs from fossil fuel combustion and biomass burning; and $MAC_{BC}(880)_{\text{fossil}}$ and $MAC_{BC}(880)_{\text{biomass}}$ are the

mass absorption cross-sections of eBC_{fossil} and the mass absorption cross-section of eBC_{biomass} at the wavelength of 880 nm respectively, which were based on the PMF results for the optical source apportionments.

2.5 Indicators for the different scales of motion

The mathematical definitions of airflow condition proposed by Allwine and Whiteman (1994) were used in this study. The definitions quantify the flow features integrally at individual stations. Three variables were quantified, namely the actual wind run distance (S) which is the scalar displacement of the wind in 24 h (i.e. the accumulated distance of the wind), the resultant transport distance (L) which is the vector displacement of the wind in 24 h (i.e. the straight line from the starting point to the end point), and the recirculation factor (R) is based on the ratio of L and S which indicates the frequency of the wind veering in 24 h. The influences of different scales of atmospheric motions were assessed based on the method proposed by Levy et al., (2010), and for this, we used wind data at 100 m above the sampling site and the wind data from 12 monitoring stations at ground level (~15m) to indicate the different scales of motions. The winds at the surface monitoring stations were expected to be more sensitive to local-scale turbulence and convection than the winds at 100 m. With less influence from the surface forces, the indicators at 100 m would be more sensitive to larger scales of motion. The equations used as follows:

$$L_{n\tau/bj} = T \left[\left(\sum_{j=i}^{i-\tau+1} u_j \right)^2 + \left(\sum_{j=i}^{i-\tau+1} v_j \right)^2 \right]^{1/2} \quad (11)$$

$$S_{n\tau/bj} = \sum_{j=i}^{i-\tau+1} (u_j^2 + v_j^2)^{1/2} \quad (12)$$

$$R_{n\tau/bj} = 1 - \frac{L_{i\tau}}{S_{i\tau}} \quad (13)$$

where T is the interval of the data (i.e., 60 min), i is the i^{th} the ending time step data, τ is the integration time period of the wind run (24 h), $i-\tau+1$ represents the data at the start time, and n is the number of monitoring stations (a total of 12 in this study). The quantities u and v are the wind vectors. Using the wind data from the 12 monitoring stations covering Baoji, the L and S values at the 12 different sites at ground level were calculated. $L_{n\tau}$ and $S_{n\tau}$ represent the resultant transport distance and the actual wind run distance at the n^{th} ($n = 1$ to 12) monitoring station at ground level; $R_{n\tau}$ is the recirculation factor at the n^{th} monitoring station which is calculated based on $L_{n\tau}$; and $S_{n\tau}$; L_{bj} , and S_{bj} are the resultant transport distance and the actual wind run distance at 100 m height above the ground. These represent the flow characteristics in higher atmosphere at the study site, and they were calculated by using the wind data at 100 m height. The recirculation factor (R_{bj}) was calculated for a height of 100 m.

As explained in Levy et al., (2010), if local-scale motions are strong and regional-scale motions are weak, the variations in winds at each station would not be likely to be uniform due to differences in local factors, and that would result in relatively large standard deviations (R_{std}) for $R_{n\tau}$. By contrast, if the local-scale motions are weak and the regional-scale motions are strong, the wind direction would be likely to be more uniform over a large area, and the R_{bj} and the R_{std} should be relatively smaller.

2.6 Self-organizing map

A self-organizing map (SOM) developed by Kohonen (1990) is a type of artificial neural network that is widely used for categorizing high-dimensional data into a few major features (Stauffer et al., 2016 and Pearce et al., 2014). In particular, this approach is widely used for categorizing different meteorological patterns (Liao et al., 2020; Han et al., 2020; Jiang et al., 2017). Unlike traditional dimension reduction methods (e.g., principal component analysis), SOM projects high-dimensional input data by non-linear projection into user-designed lower-dimensions, which are typically two-dimensional arrays of nodes

(Hewitson and Crane, 2006). The performance of SOM in classifying climatological data has been shown to be robust (Reusch et al., 2005). Competitive learning algorithms are used to train SOM, and the architecture of SOM consists of two layers; one is called the input layer and it contains the high dimensional input data. The other layer is the output layer in which the node number is the output cluster number. The working principle of SOM is to convert high dimensional data with complex correlations into lower dimensions via geometrical relationships (Ramachandran et al., 2019). After the initial random weights are generated, the input data are compared with each weight, and the best match is defined as winning. The winning node and the neighboring nodes close to the winning node will learn from the same inputs and the associated weights are updated. After multiple iterations, the network settles into stable zones of features and the weights. More detailed working principles of SOM can be found Kangas and Kohonen, (1996) and Kohonen et al., (1996).

Comparison between the input data and each weight is made by applying Euclidean distances, the best match is defined by the following equation:

$$\|x - m_c\| = \min\{\|x - m_i\|\} \quad (14)$$

where x is the input data, m_c is the best matched weight, m_i is the weights connected with the i^{th} node.

The weights are updated by following equation:

$$m_i(t + 1) = m_i(t) + h_{ci}(t)[x(t) - m_i(t)] \quad (15)$$

where the $m_i(t + 1)$ is the i^{th} weight at $t+1$ time, $m_i(t)$ is the i^{th} weight at t time, the $h_{ci}(t)$ is the neighborhood kernel defined over the lattice points at t time, and c is the winning node location.

SOM was used to categorize the daily atmospheric motions during the study period and to explore the influences of different scales of motion on source-specific eBC. Hourly averages of three sets of data (R_{std} , L_{bj} , and S_{bj}) were input into SOM. Determining the size of the output map is crucial for SOM (Chang et al 2020 and Liu et al., 2021). To reduce the subjectivity, the K-means cluster method was used for the decision-making regarding size. The similarity of each item of the input data relative to the node was measured using Euclidean distance. The iteration number was set to 2000. For each input data item, the node closest to it would “win out”. The reference vectors of the winning node and their neighborhood nodes were updated and adjusted towards the data. The “Kohonen” package in R language (Wehrens and Kruisselbrink, 2019) was used to develop the SOM model in this study.

2.7 Estimations of direct radiative effects and heating rate

The Santa Barbara DISORT Atmospheric Radiative Transfer (SBDART) model was used to estimate the direct radiative effects (DRE) induced by source-specific eBC. The model has been used in many studies to calculate the DRE caused by aerosols and BC (Pathak et al., 2010; Rajesh et al., 2018; Zhao et al., 2019). SBDART calculated DRE based on several well-tested physical models. Details regarding the model were presented in Ricchiazzi et al., (1998). The important input data included aerosol parameters, including aerosol optical depth (AOD), single scattering albedo (SSA), asymmetric factor (AF) and extinction efficiency, surface albedo, and atmospheric profile.

The aerosol parameters used in this study were derived by the Optical Property of Aerosol and Cloud (OPAC) model (Hess et al., 1998) based on the number concentrations of aerosol components. As the study was conducted in an urban region, the urban aerosol profile was used in OPAC, and it included soot (eBC), water-soluble matter (WS), and water-insoluble matter (WIS). The number concentrations of soot were derived from the mass concentrations of eBC with the default ratio ($5.99\text{E-}5 \mu\text{g m}^{-3}/ \text{particle.cm}^{-3}$) in OPAC.

The number concentrations of WS and WIS were adjusted until the modeled SSA and b_{abs} at 500nm in OPAC were close ($\pm 5\%$, see Figure S4) to those values calculated with data from the nephelometer and AE33 ($b_{\text{ext}}(520) = b_{\text{scat}}(525) + b_{\text{abs}}(520)$, $\text{SSA} = b_{\text{scat}}(525)/b_{\text{ext}}(520)$). The DRE of source-specific eBC at the top of atmosphere (TOA) and surface atmosphere (SUF) were calculated from the difference between the DREs with or without the number concentrations of the source-specific eBC under clear-sky conditions.

$$DRE_{eBC} = (F \downarrow - F \uparrow)_{\text{with } eBC} - (F \downarrow - F \uparrow)_{\text{without } eBC} \quad (16)$$

$$DRE_{eBC,ATM} = DRE_{eBC,TOA} - DRE_{eBC,SUF} \quad (17)$$

where DRE_{eBC} is the DRE of source-specific eBC, $F \downarrow$ and $F \uparrow$ are the downward and upward flux, $DRE_{eBC,ATM}$ is the DRE of the source-specific eBC for the atmospheric column, that is, the DRE at the top of the atmosphere ($DRE_{eBC,TOA}$) minus that at the surface ($DRE_{eBC,SUF}$).

“Text S1. Minimum R - squared method

The minimum R squared method developed by Wu et al., (2016) was used to separate secondary organic carbon (SOC) from the primary organic carbon (POC). The assumption behind this method is the organic carbon (OC) from non-combustion source is negligible. As explained by Wang et al., (2019), the major non-combustion source is biogenic which is mainly exists in coarse mode. Thus, the non-combustion organic carbon is considered negligible in this study. Therefore, SOC and POC can be separated by using following equations. For each date set, the ratios of OC to eBC and SOC and the R^2 between eBC and SOC can be calculated. SOC and eBC are considered independent, so the $(\text{OC}/\text{eBC})_{\text{pri}}$ should be the value obtained when the R^2 between eBC and SOC is minimum.

$$\text{POC} = (\text{OC}/\text{EC})_{\text{pri}} \times \text{EC} \quad (\text{S1})$$

$$\text{SOC} = \text{OC}_{\text{total}} - (\text{OC}/\text{EC})_{\text{pri}} \times \text{EC} \quad (\text{S2})$$

where EC in this study is eBC. The $(\text{OC}/\text{EC})_{\text{pri}}$ is the ratio in freshly emitted OC and EC from combustion sources.

The light absorption at shorter wavelengths ($< 660\text{nm}$) is not only from primary light absorbing substances but also from the secondary organic carbon (Wang et al., 2019). The assumption for this method is that the light absorption caused by non-combustion sources is negligible. As mentioned above, most of the biogenic BrC is in coarse mode. Another common light absorbing substance is the Fe_2O_3 in the dust, but the impact of that should be limited because the absorption from Fe_2O_3 in the dust has been reported to be much smaller than that from BC (Ramachandran and Kedia, 2010). Thus, to separate the secondary light absorption ($b_{\text{abs}}(\lambda)_{\text{secondary}}$) from the primary light absorption ($b_{\text{abs}}(\lambda)_{\text{primary}}$), a BC-tracer method coupled with a minimum R-squared method was used. The equations used for the calculation are follows:

$$b_{\text{abs}}(\lambda)_{\text{secondary}} = b_{\text{abs}}(\lambda) - \left(\frac{b_{\text{abs}}(\lambda)}{\text{BC}}\right)_{\text{pri}} \times \text{BC} \quad (\text{S3})$$

$$b_{\text{abs}}(\lambda)_{\text{primary}} = b_{\text{abs}}(\lambda) - b_{\text{abs}}(\lambda)_{\text{secondary}} \quad (\text{S4})$$

Where $b_{\text{abs}}(\lambda)$ is the light absorption at different wavelengths ($\lambda=370\text{nm}$, 470nm , 520nm , 590nm , 660nm) measured by AE33, BC is the eBC measured by AE33 at a wavelength of 880nm . The $\left(\frac{b_{\text{abs}}(\lambda)}{\text{BC}}\right)_{\text{pri}}$ is the ratio of the primary light absorption to the BC mas concentration from combustion sources.

Text S2. Cluster analysis of air-mass trajectories

Back trajectories were calculated by using Hybrid Single-Particle Lagrangian Integrated Trajectory (HYSPLIT) model (Draxler and Hess, 1998) developed by the Air Resource Lab (ARL) of the National Oceanic and Atmospheric Administration (NOAA). The model can predict the position of air mass by using mean wind. The back-in-time positions are calculated by reversing the advection equation (Draxler and Hess, 1997). The calculation requires the mean wind, for calculating trajectories, only advection is considered (Stein et al., 2015). The basic equations for trajectory calculation in HYSPLIT are as follows:

$$P'(t + \Delta t) = P(t) + V(P, t) \times \Delta t \quad (S5)$$

$$P(t + \Delta t) = P(t) + 0.5 \times [V(P, t) + V(P', t + \Delta t)] \times \Delta t \quad (S6)$$

Where $P(t)$ is the initial position, $P'(t + \Delta t)$ is the first guess position, V is the average velocity, t is the time, Δt is the time step.

A large number of 24 h trajectories (793) that were retrieved for the study period showed diverse pathways, so in order to find out the representative pathways for those trajectories, a cluster analysis based on an angle-based distance statistics method was conducted. Compared with Euclidean distance, angle-based distance statistics method focuses on the direction of air mass instead of the speed. The angle-based distance statistics method is defined by following equations (Sirois and Bottenheim, 1995):

$$d_{12} = \frac{1}{2} \sum_{i=1}^n \cos^{-1} \left(0.5 \times \frac{A_i + B_i - C_i}{\sqrt{A_i B_i}} \right) \quad (S7)$$

$$A_i = (X_1(i) - X_0)^2 + (Y_1(i) - Y_0)^2 \quad (S8)$$

$$B_i = (X_2(i) - X_0)^2 + (Y_2(i) - Y_0)^2 \quad (S9)$$

$$C_i = (X_2(i) - X_1(i))^2 + (Y_2(i) - Y_1(i))^2 \quad (S10)$$

Where d_{12} is the average angle between the two backward trajectories, varying between 0 and π ; X_0 and Y_0 are the position of the receptor site; and X_1 (Y_1) and X_2 (Y_2) are the backward trajectories 1 and 2, respectively. In this study, three clusters were chosen as representative of the backward trajectory clusters based on the total spatial variance (TSV) value. The simulation was conducted using the GIS-based TrajStat software (Wang et al., 2009)."

The discussion section could be strengthened by comparing this work with other studies in similar topographic conditions.

Response: We have reviewed studies on BC pollution and the total DRE of BC at other river valley sites and compared them with this study. The revised text is as follows:

"The mean values of eBC_{fossil} and eBC_{biomass} were $2.46 \mu\text{g m}^{-3}$ and $1.17 \mu\text{g m}^{-3}$, respectively. The averaged total eBC mass concentration (\pm standard deviation) was $3.63 \pm 2.73 \mu\text{g m}^{-3}$, and the eBC ranged from varying from 0.39 to $12.73 \mu\text{g m}^{-3}$ during the study period, The averaged mass concentration was comparable to that in Lanzhou, another river valley city in China, that was sampled in the same season (5.1 ± 2.1 , Zhao et al., 2019). The lowest value is comparable to other river valley regions such as in Retje in India (Glojek et al.,

2022) or in Urumqi River Valley in China (Zhang et al., 2020), however even the highest concentration was much lower than that in other urban regions (Table S5).”

“Figure 5a shows the DREs at top of the atmosphere ($DRE_{eBC, TOA}$), surface ($DRE_{eBC, SUR}$), and the whole atmosphere ($DRE_{eBC, ATM}$) of eBC_{fossil} and $eBC_{biomass}$. The $DRE_{eBC, TOA}$ and $DRE_{eBC, SUR}$ of eBC were 13 W m^{-2} and -22.9 W m^{-2} , which were lower than that reported in Lanzhou (21.8 W m^{-2} and -47.5 W m^{-2} for $DRE_{eBC, TOA}$ and $DRE_{eBC, SUR}$) – which is another a river valley city in China (Zhao et al., 2019). This could be due to fact that the eBC mass concentration in Baoji was lower than in Lanzhou (Table S5). As for the $DRE_{eBC, TOA}$ and $DRE_{eBC, SUR}$ per an unit mass of BC, the results of the two studies were comparable.”

Table R1 Mean (range) BC mass concentration in river valley sites worldwide

Reference	BC concentration ($\mu\text{g m}^{-3}$)	Season	Topographic conditions	Altitude	Station type	Year
This study	3.63 ± 2.73 (0.39~12.73)	November~December (winter)	river valley	450 to 800 m a.s.l. ^a	urban	2018
Glojek et al., (2020)	0.9~40	December~January (winter)	river valley	715 m a.s.l.	rural	2017-2018
Zhao et al. (2015)	25 ± 11	January (winter)	river valley	410 m a.s.l.	urban	2013
Barman and Gokhale (2019)	20.58~22.44	Winter	river valley		urban	2016-2017
Zhang et al., 2020	0.102~1.525	Winter	river valley	2130 m a.s.l.	rural	2016-2017
Chakrabarty et al., (2012)	9~41	January~February (winter)	river valley		urban	2011
Zhao et al. (2019)	5.1 ± 2.1	December~January (winter)	river valley		urban	2018
Tiwari et al., 2016	8.19 ± 1.39	December-February (winter)	river valley	55 m a.s.l.	urban	2013-2014

^aasl stands for “above sea level.”

References:

Barman, N., and Gokhale, S., Urban black carbon - source apportionment, emissions and long-range transport over the Brahmaputra River Valley, *Science of the Total Environment*, 693, 133577, <https://doi.org/10.1016/j.scitotenv.2019.07.383>, 2019

Chakrabarty, R., Garro, M., Wilcox, E., and Moosmuller, H., Strong radiative heating due to wintertime black carbon aerosols in the Brahmaputra River Valley, *Geophysical Research Letters*, 39, L09804, <https://doi.org/10.1029/2012GL051148>, 2012.

Glojek, K., Močnik, G., Alas, H., et al., The impact of temperature inversions on black carbon and particle mass concentrations in a mountainous area, *Atmos. Chem. Phys.*, 22, 5577–5601, <https://doi.org/10.5194/acp-22-5577-2022>, 2022.

Zhang, X., Li, Z., Ming, J., and Wang, F., One-year measurements of equivalent black carbon, optical properties, and sources in the Urumqi River Valley, Tien Shan, China, *Atmosphere*, 11, 478, <https://doi.org/10.3390/atmos11050478>, 2020.

Zhao, S., Yu, Y., Yin, D., et al., Concentrations, optical and radiative properties of carbonaceous aerosols over urban Lanzhou, a typical valley city: Results from in-situ observations and numerical model, *Atmospheric Environment*, 213, 470–484, <https://doi.org/10.1016/j.atmosenv.2019.06.046>, 2019.

Zhao, S., Tie, X., Cao, J & Zhang, Q. (2015), Impacts of mountains on black carbon aerosol under different synoptic meteorology conditions in the Guanzhong region, China. *Atmospheric Research*, 164-165, 286-296. <http://dx.doi.org/10.1016/j.atmosres.2015.05.016>

Tiwari, S., Kumar, R., Tunved, P., Singh, S., and Panicker, A., Significant cooling effect on the surface due to soot particles over Brahmaputra River Valley region, India: An impact on regional climate, 2016, *Science of the Total Environment*, 562, 504–516, <http://dx.doi.org/10.1016/j.scitotenv.2016.03.157>, 2016.

The writing should be improved, I have suggested a few technical corrections in a specific section at the end.

Response: As suggested, we have had this manuscript polished by a native English speaker.

Specific comments:

L30: What type of “change” between a mass concentration and a radiative effect is expected? I am not sure the word “change” conveys your meaning.

Response: By “change” we meant that the changes in BC mass concentrations for the different scales of motions were not of the same magnitude as the changes in BC DRE. More specifically, we took LD as a base case to calculate the difference between the average BC mass concentrations (or average DRE) versus other cases (LSTW, LWRS and RD). Clearly the eBC_{fossil} and $eBC_{biomass}$ concentrations decreased more than the corresponding DRE did (Table R2). This indicates that the DREs per unit mass of BC were variable (Table R3).

To avoid confusion, we revised it into “Similar to the mass concentrations, the DREs of the two types of eBC were both lower when the regional scale of motions were greater than the local ones. However, the changes in mass concentrations and DREs were not proportionate because the regional-scale of motions carried the fresh BC away from the local site but brought the aged BCs to the site from the upwind regions. As a result, the DRE efficiency of eBC was ~1.5 times higher when the regional scale of motion was stronger.”

Table R2 The change of mass concentration of different eBCs and their DREs

Atmospheric motion category	Change of mass concentration of eBC_{fossil}	Change of mass concentration of $eBC_{biomass}$	Change of $DRE_{eBC_{fossil}, ATM}$	Change of $DRE_{eBC_{biomass}, ATM}$
LD	-	-	-	-
LSRW	9.4%	30.3%	5.7%	-2.9%
LWRS	30.2%	43.4%	29.3%	23.1%
RD	45.1%	38.8%	34.6%	29.0%

Table R3. Direct radiative forcing efficiencies for equivalent black carbon (eBC) from fossil fuel combustion (eBC_{fossil}) and the eBC from biomass burning ($eBC_{biomass}$) under four atmospheric motion categories

Atmospheric motion category	DRE _{eBCfossil, ATM} efficiency ((W m ⁻²)/(μg m ⁻³))	DRE _{eBCbiomass, ATM} efficiency ((W m ⁻²)/(μg m ⁻³))
Local scale dominance (LD)	10.2 ^a ± 4.2 ^b	10.3 ± 4.4
Local scale strong and regional scale weak (LSRW)	10.6 ± 5.7	10.2 ± 5.8
Local scale weak and regional scale strong (LWRS)	13.5 ± 6.7	14.7 ± 8.1
Regional scale dominance (RD)	15.6 ± 8.9	15.5 ± 8.4

a and b: Mean ± Standard deviation

L37-38: “the second strongest light-absorbing substance in the atmosphere after CO₂”. This wording is confusing since it seems an intrinsic property of BC whatever its concentration level. Besides it is clearly related to (1) its climate forcing ability and (2) human emissions only, by Bond et al. (2013) which state that “We estimate that black carbon, with a total climate forcing of +1.1 W m⁻², is the second most important human emission in terms of its climate forcing in the present-day atmosphere; only carbon dioxide is estimated to have a greater forcing.” (abstract) or “Our best estimate of black carbon forcing ranks it as the second most important individual climate-warming agent after carbon dioxide” (in 1.2.12 Policy implications). This sentence should thus be revised accordingly.

Response: Thanks for pointing this out, we have revised this sentence:

“Black carbon (BC) is produced by the incomplete combustion of biomass and fossil fuels. The BC aerosol has a strong light absorption capacity and can cause heating of the atmosphere. In fact, BC is widely recognized as one of the most important short-lived climate forcers (IPCC, 2021).”

In the abstract, the relevant sentence has also been revised into:

“Black carbon (BC) is one of the most important short lived climate forcers, and atmospheric motions play an important role in determining its mass concentrations of pollutants.”

L60: “scale (it is atmosphere phenomena) ranges”. I do not understand what the mention in brackets refers to?!

Response: We have deleted this—it was a mistake.

L62: I do not understand how an atmospheric dynamic feature (the local scale of motion) is eventually controlled by the concentration levels of BC?! Besides the land roughness, it can be influenced by thermals, turbulence, etc.

Response: We agree with reviewer that thermals and other factors cause local scales of motion, but the variations in the BC mass concentrations also can induce thermal differences horizontally and vertically. The horizontal temperature variations can give rise to horizontal pressure differences, which result in atmospheric motions (Oke, 1988). BC concentration also can impact the temperature structure of the atmosphere and cloud microphysical properties, the latter of which also can impact the temperature (IPCC, 2021). In this way, differences of BC mass concentrations between different locations can lead to atmospheric motions.

Reference:

Oke, T., *Boundary Layer Climates*, 2nd edition, Taylor & Francis e-Library, 2002.

IPCC: *Climate Change 2021: The Physical Science Basis. Contribution of Working Group I to the Sixth Assessment Report of the Intergovernmental Panel on Climate Change* [Masson-Delmotte, V., P. Zhai, A. Pirani, S.L. Connors, C. Péan, S. Berger, N. Caud, Y. Chen, L. Goldfarb, M.I. Gomis, M. (eds)], <https://reliefweb.int/report/world/climate-change-2021-physical-science-basis>, 2021

IPCC: *Climate Change 2021: The Physical Science Basis. Contribution of Working Group I to the Sixth Assessment Report of the Intergovernmental Panel on Climate Change* [Masson-Delmotte, V., P. Zhai, A. Pirani, S.L. Connors, C. Péan, S. Berger, N. Caud, Y. Chen, L. Goldfarb, M.I. Gomis, M. (eds)], <https://reliefweb.int/report/world/climate-change-2021-physical-science-basis>, 2021

L72-79: The authors mention the specific case of atmospheric dynamics in the context of a valley site surrounded by mountains. I am surprised not to find a word about temperature inversions which are very common in winter in such environments and have a tremendous impact on trapping pollution in valleys. See for instance Glojek et al. (2022), <https://doi.org/10.5194/acp-22-5577-2022>.

Response: We agree with reviewer that temperature inversions in river valley region are not uncommon and can exacerbate pollution problems. Indeed, this happens often in winter in Guanzhong Plain (Bei et al., 2016). Accordingly, we have added this background information into the description of the topography of the river-valley as follows:

“Topography also plays an important role in air pollution (Zhao et al., 2015). River-valley topography is complicated, and it can have a considerable influence on air pollution and synoptic patterns of flow (Green et al., 2016; Carvalho et al., 2006). The pollution levels at cities in river-valleys are not only influenced by general atmospheric dynamics but also strongly impacted by the local-scale of dynamics (Brulfert et al., 2006). Surface albedo and surface roughness are affected by the complex topography of river-valley regions, and those physical factors can affect circulation causing changes in pollutant mass concentrations (Wei et al., 2020). Mountains also significantly affect pollution, and once pollutants are generated or transported into the river-valley regions, their dispersal can be impeded by the blocking effect of the mountains. Instead of being dispersed, they can be carried by the airflows over the mountains to converge at the bottom of the valley and increase the pollutants along the river (Zhao et al., 2015). In this way, pollutants can accumulate in valleys and spread throughout the area, thereby aggravating pollution. In addition, temperature inversions commonly form in river-valleys during the winter, and that, too, can aggravate pollution problems (Glojek et al., 2022 and Bei et al., 2016).”

Reference:

Bei, N., Li, G., Huang, R., Cao, J., Meng, N., Feng, T., Liu, S., Zhang, T., Zhang, Q., and Molina, L.: Typical synoptic situations and their impacts on the wintertime air pollution in the Guanzhong basin, China, *Atmos. Chem. Phys.*, 16, 7373–7387, <http://dx.doi.org/10.5194/acp-16-7373-2016>, 2016.

Glojek, K., Močnik, G., Alas, H., Cuesta-Mosquera, A., Drinovec, L., Gregorič, A., Ogrin, M., Ježek, I., Müller, T., Rigler, M., Remškar, M., Pinxteren, D., Herrmann, H., Ristorini, M., Merkel, M., Markelj, M., Wiedensohler, A.: The impact of temperature inversions on black carbon and particle mass concentrations in a mountainous area, *Atmos. Chem. Phys.*, 22, 5577–5601, <https://doi.org/10.5194/acp-22-5577-2022>, 2022.

L87: The description of the research site and its surroundings is too brief. No mention of any altitude (site, surrounding mountains), which is a crucial parameter. The authors should provide a more detailed map of the city and the main local expected sources of Black Carbon (highway, residential areas, industries, etc.), as well as the 12 monitoring stations mentioned later in the text. It would also be helpful to know about the local wind rose over the different seasons, as well as basic meteorological data (temperature, RH profiles; precipitation patterns).

Response: We revised the site description to include the altitude, main local sources of BC, population density and so on. The seasonal meteorological data for Baoji is listed in Table R4 and the seasonal local wind roses are provided in Figure R1. The table and figure have been included in the supplementary materials. The revised site description is now reads:

“Baoji is a typical river-valley city, located at the furthest west of the Guanzhong Plain, at an altitude from 450 to 800 m a.s.l. (Figure S1), Baoji has a complex topography and often suffering from severe pollution in winter. It is surrounded by mountains to the south, west and north, with the Weihe River as the central axis extending eastward. The shape can be viewed as a funnel, with large opening to east. The Qinling peaks and the flat Weihe Plain are the main landforms of Baoji. The main peak of the Qinling Mountains is 3,767 m a.s.l. and it is the highest mountain in the eastern part of mainland China. This terrain causes divergent flow at local scales, which can impact pollution levels (Wei et al., 2020). Baoji also is an important railway intersection in China, connecting six railways to the north-west and southwest China. Pollutant levels can be high and pollutants are not easy to be dispersed in the city due to its special topographic conditions, dense population (total population of 0.341 million, with 63.5% population living in the downtown area and population density of 6003 people per km² in 2019 (<http://tjj.shaanxi.gov.cn/upload/2021/zk/indexch.htm> and <https://data.chinabaogao.com/hgshj/2021/042053X932021.html>), and impacts from major highway and railway networks.

The sampling site was on the rooftop of a building at Baoji University of Arts and Sciences (34°21'16.8"N, 107°12'59.6"E, 569 m a.s.l.) surrounded by commercial and residential buildings, highways, and a river, there were no major industrial emission sources nearby. The main sources of BC in Baoji were the domestic fuel (coal and biomass) burning as well as the motor vehicle emissions (Zhou et al., 2018; Xiao et al., 2014). Open fire also can be sources for BC, but there were limited fire found scattered around the site (Figure S2). The meteorological conditions at Baoji for the four seasons are listed in Table S1, and the wind roses for the different seasons are shown in Figure S3(data are from the Meteorological Institute of Shaanxi Province).”

Table R4. The seasonal meteorological data of Baoji

Season	Temperature (°C)	Relative humidity (%)	Precipitation in last hour (mm)
Winter	2.7	60.6	0.025
Spring	11.5	54.9	0.042
Summer	23.7	67.1	0.139
Autumn	20.2	67.0	0.074

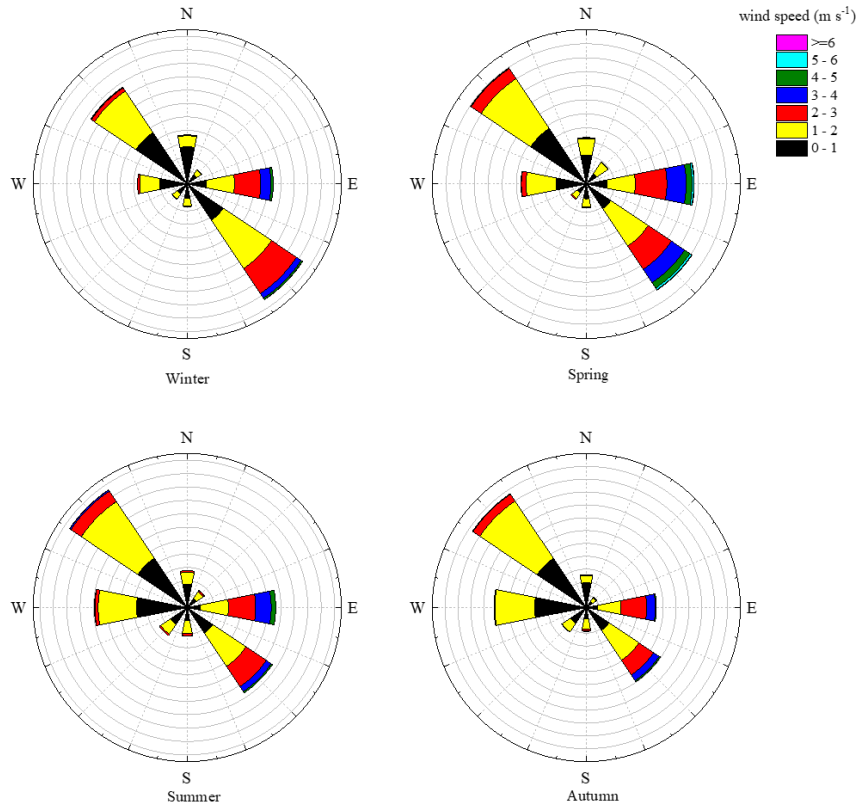


Figure R1 Seasonal wind roses for Baoji.

We also have updated the map of the region in supplementary materials. The new map looks like:

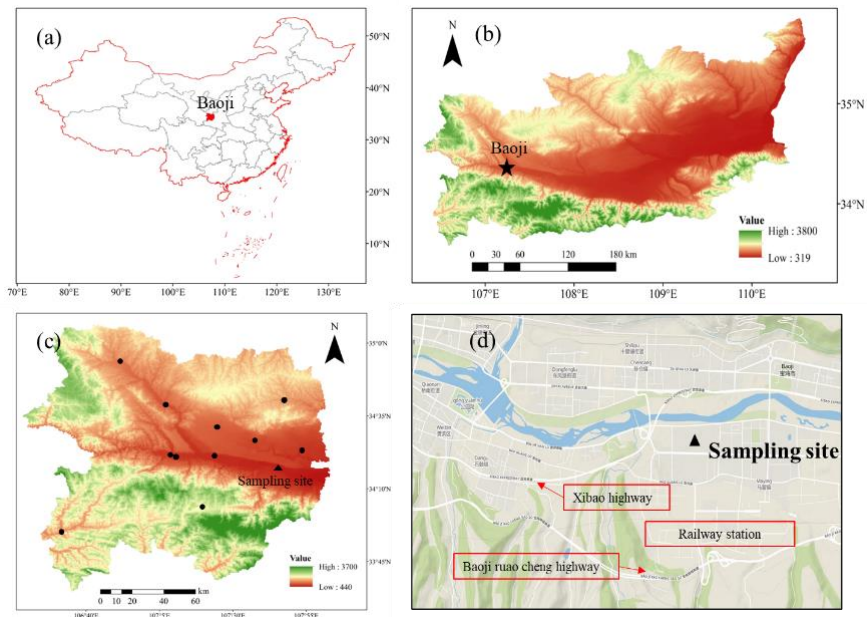


Figure R2. A map of the research site; (a) map of China—the red shape is the location of Baoji, (b) a map of the Guanzhong Plain, the black star represents the location of Baoji; (c) a map of Baoji City, the black dots and the black triangle represent 12 stations and the triangle is the location of sampling site, (d) a map of the sampling site.

L101: The time resolution of AE33 aethalometers can either be 1 min or 1 s. Do you mean you used 5-min averages of the 1-min data?

Response: The original data had 1-min time resolution. This has been corrected:

“eBC and the absorption coefficients (b_{abs}) at 370, 470, 520, 590, 660, 880, and 950 nm wavelength were measured using an AE33 aethalometer (Magee Scientific, Berkeley, CA, USA) equipped with a PM_{2.5} cut-off inlet (SCC 1.829, BGI Inc. USA) that had a time resolution of 1 min.”

L105-106: What type of quartz filter was used? The correction factor is dependent on the filter model.

Response: We double checked with the one of the coauthors about the tape and the C value used for this sampling. The tape is PN8060. We reset the C value to 1.39 instead of 2.14. Thanks so much for spotting this omission. We corrected this in the revised version.

“The quartz filter (PN8060) matrix scattering effect was corrected by using a factor of 1.39.”

L133: What is the spatial resolution of the GDAS meteorological data?

Response: The spatial resolution of GDAS data is 1°×1°. We have added the resolution into the manuscript and provide a table with data and the main parameters used for the HYSPLIT model (Table R5).

“The data used for the Hybrid Single-Particle Lagrangian Integrated Trajectory (HYSPLIT) model was downloaded from Global Data Assimilation System and it had a resolution of 1°×1° (GDAS, <https://www.ready.noaa.gov/gdas1.php>). The data and main parameters used in trajectory model are listed in Table S2.”

Table R5. Data and parameters used in HYSPLIT model

Items	Data/parameters
Model	HYSPLIT
Meteorological data	GDAS data, 1° × 1°, 23 vertical levels, 3 hourly
Backward period	24h
Footprint level	100 m above the ground
Receptor site location	34°21'16.8"N, 107°12'59.6"E

L162: The PMF methodology is described in section 2.3 for its classical use with mass concentrations of chemical species. Here it is used for optical source apportionment and therefore it should be explained how (concentrations are being replaced by what?) as well as the uncertainty calculation in that case.

Response: The use of the input data follows equation (R1)

$$X_{ij} = \sum_{k=1}^p g_{ik}f_{kj} + e_{ij} \quad (R1)$$

where X_{ij} denotes the input data matrix; p is the number of sources selected in the model; g_{ik} denotes the contribution of the k^{th} factor to the i^{th} input data; f_{kj} represents the k^{th} factor's profile of the j^{th} species; and e_{ij} represents the residual. Both g_{ik} and f_{kj} are non-negative.

As shown in the equation R1, the balance (mass balance for chemical data, total absorption balance for absorption data) isn't be violated by using a mixed input matrix X because each X_{ij} is independent from the others. PMF analysis is not degraded a priori by using joint matrices containing different dimensions/units (Forello et al., 2019 and reference therein). Putting data with different units in X means that matrix G (g_{ik}) is unitless and the corresponding column data in F (f_k) will have the same unit as the total values you into X (Paatero, 2018).

In addition, we were not interested in the total particulate mass which would satisfy the condition that the mass is equal to the sum of the mass of each chemical species. Instead, we focused only on the relationship between EC and light absorption coefficients to retrieve AAE values. We used chemical species only as tracers for different emission sources to help identify the factors. Thus, we simply use a joint matrix X[Y Z] where Y represents the part of the matrix for chemical species, Z represents the part of the matrix for light absorption coefficients.

The uncertainty of the input data was calculated by the following equation recommended in EPA PMF5.0 user guideline:

$$\text{Unc} = \sqrt{(\text{Error Fraction} \times \text{concentration})^2 + (0.5 \times \text{MDL})^2} \quad (\text{R2})$$

$$\text{Unc} = \frac{5}{6} \times \text{MDL} \quad (\text{R3})$$

where MDL is the minimum detection limit of different input data. When the concentration of species was higher than MDL then equation R2 was used otherwise equation R3 was used.

The error fraction for the offline measured data was the analytical uncertainty which in this study was taken to be the difference between replicate analyses of the same sample. The MDL was used based on the MDL of each chemical species as measured by the analytical instrumentation. For light absorption coefficients, the error fraction used was the measurement uncertainty of AE33. The uncertainty was estimated about 10% including changes in filter scattering caused due to aerosol loading, underestimation of source signals with increased filter loading, sample flow rate, filter spot area, and detector response (Rajesh and Ramachandran, 2019). Thus, we used 10% for light absorption coefficients for all wavelengths. The MDL of b_{abs} we used the value of 0.039 M m^{-1} which is converted from the reported BC MDL of AE33 ($0.005 \mu\text{g m}^{-3}$) in Rajesh and Ramachandran (2018).

To make the calculation clear, we have revised section 2.3, which can be seen in the response above.

Reference:

Forello, A. C., Bernardoni, V., Calzolari, G., Lucarelli, F., Massabo, D., Nava, S., Pileci, R. E., Prati, P., Valentini, S., Valli, G., and Vecchi, R.: Exploiting multi-wavelength aerosol absorption coefficients in a multi-time resolution source apportionment study to retrieve source-dependent absorption parameters, *Atmos. Chem. Phys.*, 19, 11235-11252, 10.5194/acp-19-11235-2019, 2019.

Paatero, P.: Interactive comment on "Receptor modelling of both particle composition and size distribution from a background site in London, UK – the twostep approach" by David C. S. Beddows and Roy M. Harrison, <https://doi.org/10.5194/acp-2018-784-RC2>, 2018.

Rajesh, T., and Ramachanran, S., Black carbon aerosol mass concentration, absorption and single scattering albedo from single and dual spot aethalometers: Radiative implications, *Journal of Aerosol Science* 119, 77–90, <https://doi.org/10.1016/j.jaerosci.2018.02.001>, 2018.

L184: Is equation 13 correct? Both L175 and L188-189 describe R as the ratio between L and S but this does not correspond to the expression.

Response: We apologize for the inaccurate expression. The “R” on line 175 is the R defined in equation 13. We have corrected the description of the R in line 175. Now it consistent with the equation 13:

“Three variables were quantified, namely the actual wind run distance (S) which is the scalar displacement of the wind in 24 h (i.e. the accumulated distance of the wind), the resultant transport distance (L) which is the vector displacement of the wind in 24 h (i.e. the straight line from the starting point to the end point), and the recirculation factor (R) is based on the ratio of L and S which indicates the frequency of the wind veering in 24 h.”

L206: What is the time resolution of the three sets of data? Are you using hourly averages?

Response: Yes, we used hourly averaged data. To make this clear, we added the time resolution into the sentence:

“Hourly averages of three sets of data (R_{std} , L_{bj} , and S_{bj}) were input into SOM. Determining the size of the output map is crucial for SOM (Chang et al 2020 and Liu et al., 2021).”

L303-318: I would suggest to include the four different average values ($L(bj)$, $S(bj)$, $R(bj)$ and $R(std)$) for the four motion categories in Table 1 as well, and not repeat all the values in this paragraph but rather focus on the comparison and the interpretation.

Response: Thanks for the suggestion, we have revised this part in 3.2 section to make this section more concise and readable. The revised version is:

“The K-means results showed that the four-category solution was appropriate for interpretation as explained above (see also Figure S10). Thus a 2×2 map size was used for the self organizing map (SOM). The four featured atmospheric motion categories given by SOM (Figure S11) were identified as follows (feature values are in Table 1):

1. Local-scale dominance (LD): This category featured high R_{bj} and R_{std} . As described in section 2.5, high R_{std} indicates greater divergence of R at the 12 stations due to the strong influence of local-scale turbulence and convection. L_{bj} and S_{bj} were shorter than 130 km implying stagnation (Allwine and Whiteman, 1994).
2. Local-scale strong and regional-scale weak (LSRW): For this group, L_{bj} and S_{bj} were longer than those for LD, and R_{std} was slightly lower than that in LD.
3. Local-scale weak and regional-scale strong (LWRS): As the values suggest, both R_{bj} and R_{std} were lower than those in LD and LSRW, especially R_{bj} . This suggests the winds veered less frequently and the differences of R found in 12 stations were smaller than in the two situations above. This situation shows that the influence of the regional-scale motion was greater than that for the previous two categories.
4. Regional-scale dominance (RD): In this category, wind direction at the study site was nearly uniform (extremely low R_{bj}) suggesting good ventilation (Allwine and Whiteman, 1994). The differences among R found at the 12 stations were even smaller than for the LWRS group, implying a strong increased influence of regional-scale motions. Indeed, the influence of regional-scale motions far outweighed the

local ones for this category, and therefore, this group was considered to be dominated by strong regional-scale motions.”

Table R6. The mass concentration of eBC from fossil fuel combustion (eBC_{fossil}) and eBC from biomass burning (eBC_{biomass}) associated with different clusters under four featured atmospheric motions

Motion category	Local scale dominance (LD) (40%)				Local scale strong and regional scale weak (LSRW) (17%)			
	Cluster 1	Cluster 2	Cluster 3	Total average	Cluster 1	Cluster 2	Cluster 3	Total average
	$L_{bj} = 70.9 \text{ km}, S_{bj} = 107.8 \text{ km}, R_{bj} = 0.35, R_{std} = 0.25$				$L_{bj} = 106.9 \text{ km}, S_{bj} = 164.8 \text{ km}, R_{bj} = 0.33, R_{std} = 0.23$			
Trajectory percentage (%)	45	52	3	100	56	33	11	100
eBC _{fossil} ($\mu\text{g m}^{-3}$)	$2.82^a \pm 1.59^b$	3.2 ± 1.73	3.64 ± 0.67	3.08 ± 2.07	2.42 ± 1.00	3.43 ± 1.17	2.89 ± 1.00	2.79 ± 1.73
eBC _{biomass} ($\mu\text{g m}^{-3}$)	1.34 ± 1.07	1.72 ± 1.29	0.67 ± 0.87	1.52 ± 1.19	1.0 ± 0.85	1.17 ± 0.84	1.00 ± 0.64	1.06 ± 0.83

L_{bj} —resultant transport distance, S_{bj} —actual wind run distance at 100 m, R_{bj} —recirculation factor at 100 m, R_{std} —standard deviation for recirculation factor. a and b: Mean \pm Standard deviation.

Table R6 (continued)

Motion category	Local scale weak and regional scale strong (LWRS) (14%)				Regional scale dominance (RD) (29%)			
	Cluster 1	Cluster 2	Cluster 3	Total average	Cluster 1	Cluster 2	Cluster 3	Total average
	$L_{bj} = 159 \text{ km}, S_{bj} = 183.4 \text{ km}, R_{bj} = 0.13, R_{std} = 0.20$				$L_{bj} = 235.6 \text{ km}, S_{bj} = 246.4 \text{ km}, R_{bj} = 0.05, R_{std} = 0.18$			
Trajectory percentage (%)	42	22	36	100	41	20	39	100
eBC _{fossil} ($\mu\text{g m}^{-3}$)	$1.32^a \pm 0.67^b$	2.02 ± 0.73	3.16 ± 1.19	2.15 ± 1.62	1.00 ± 0.64	1.02 ± 0.88	2.75 ± 1.26	1.69 ± 1.36
eBC _{biomass} ($\mu\text{g m}^{-3}$)	0.67 ± 0.49	0.73 ± 0.47	1.19 ± 0.60	0.86 ± 0.58	0.64 ± 0.63	0.87 ± 0.69	1.26 ± 0.68	0.93 ± 0.72

L_{bj} —resultant transport distance, S_{bj} —actual wind run distance at 100 m, R_{bj} —recirculation factor at 100 m, R_{std} —standard deviation for recirculation factor. a and b: Mean \pm Standard deviation.

L341-344: Are emission inventories available to support the assumption that eBC from biomass burning is more regional than eBC from fossil fuel combustion? L388: A similar conclusion as above is reached here using the back trajectory cluster analysis.

Response: We thank reviewer for this suggestion. We considered using emission inventories to investigate this, however to our knowledge, the available emission inventory is Multi-resolution Emission Inventory for China (MEIC) which contains 6 emission categories (stationary combustion, industrial processes, mobile source, agriculture source, and residential source). We currently do not have access to a detailed source section (e.g. the individual biomass burning source and fossil fuel combustion source) inventory, which is what would be most helpful. Thus, it is not possible to show the source of biomass burning and fossil fuel combustion in an inventory map.

Non-parametric wind regression plots on these two variables could also be informative to assess the local vs. regional influence. See for instance: Gu et al. <https://www.sciencedirect.com/science/article/pii/S0160412019342369> or Pandey et al.: <https://link.springer.com/article/10.1007/s10661-022-09879-9>

Response: As suggested, we have drawn the non-parametric wind regression plots for eBC_{biomass} and eBC_{fossil}. As shown in Figure R3, during the night, the eBC_{biomass} was higher when the wind speed was faster, but in contrast, eBC_{fossil} was higher when the wind was slower. This indicates that during night, the emission sources of eBC_{biomass} were located further than the sources of eBC_{fossil}, which explains why the mass concentrations of eBC_{biomass} did not decrease when the influence of regional-scale atmospheric motions was stronger. We have added this figure to the supplementary materials.

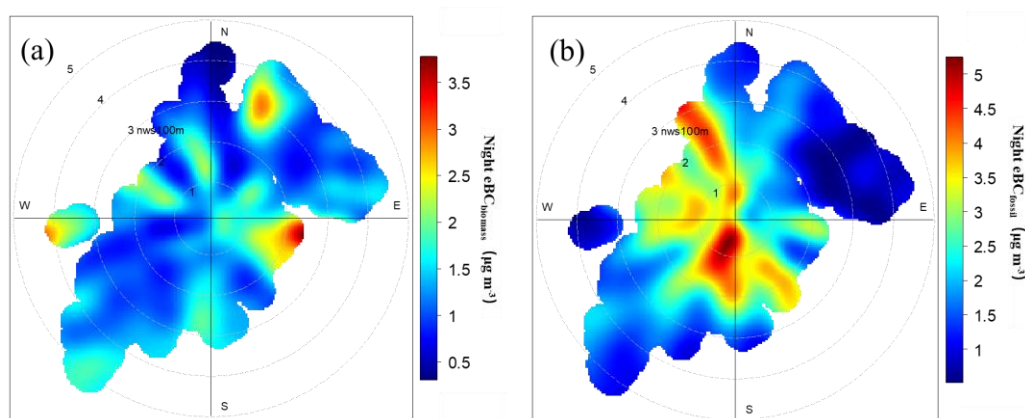
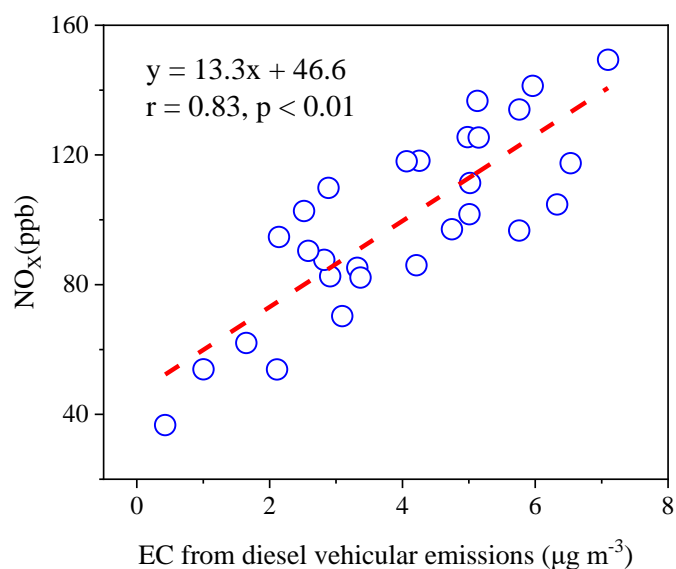


Figure R3 Non-parametric wind regression plots for eBC_{biomass} (a) and eBC_{fossil} (b) at night. The radial and tangential axes represent the wind direction (°) and speed (m s⁻¹), respectively, and nws100 m represents the night wind speed 100 m above ground level.

Supplementary Information

Figure S5: eBC(diesel) is actually EC from the PMF factor attributed to diesel vehicular emissions if I understand correctly what is written in the main text (L248). I do not think it should be considered equivalent to an eBC(diesel) which is confusing with eBC(fossil).

Response: We thank the reviewer pointing this out. It should be EC not eBC. We apologize for this mistake. The correction has been made:

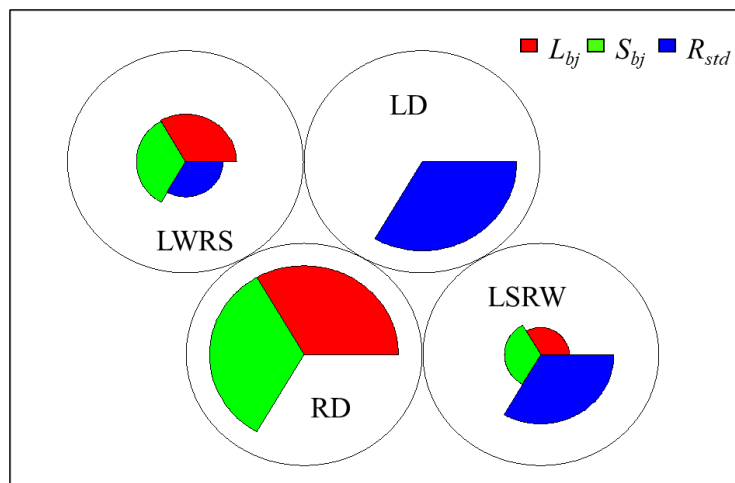


FigureR4. Linear regression of the daily averaged NO_x versus the daily averaged elemental carbon (EC) emitted from diesel vehicular emissions. The red line is the linear fit.

Figure S8: The caption is not very informative. Do L24h and S24h correspond to L_{bj} and R_{bj} mentioned in the main text. Being not familiar with the SOM approach, it is hard to figure out what this represents and how to interpret it.

Response: We agree with reviewer. The L24h and S24h correspond to L_{bj} and S_{bj} . We have updated the names to make them consistent with the main text. The averaged L_{bj} , S_{bj} and R_{std} of the four categories were calculated based on this SOM cluster.

To make this figure easier to interpret, we have added some explanation under the figure as follows:



FigureR5. The result of the self-organizing map, sectorial shape represents each variable (L_{bj} , S_{bj} and R_{std}), the bigger the size the larger this variable. The four circles with the sectorial color together indicate the features of the four motion categories. The bottom left circle means high L_{bj} and S_{bj} but low R_{std} , which

indicates the feature of regional scale dominance (RD) category. The bottom right represents the high R_{std} but relatively low L_{bj} and S_{bj} indicating local-scale strong and regional scale weak (LSRW). The upper left represents local scale weak and regional-scale strong (LWRS) and the upper right represent local scale dominance (LD).

Technical corrections (list non-exhaustive):

L32: *“It highlights”*. Do you mean *“This study emphasizes the fact that”*? (or something along that line)

Response: Yes, we do. We changed the wording:

“The finding that the DRE efficiency of BC increased during the regional transport suggested significant consequences in regions downwind of pollution sources and emphasizes the importance of regionally transported BC for potential climatic effects.”

L54: *“Local concentrations of BC are”*

Response: Correction has made.

“The concentrations of BC are controlled by local emissions and regional transport, but meteorological conditions also are important because they affect both transport and removal.”

L55: *“predictable at to some degree”*. Delete *“at”*.

Response: Correction has made.

“Normally, local emission in urban areas are predictable to some degree because those emission sources are mainly anthropogenic and the concentrations of pollutants follow the diurnal patterns driven by anthropogenic activities.”

L56: *“the concentration of pollutants follows”*

Response: Correction has made, see the response above.

L57: *“multiple” instead of “multiply”*

Response: We corrected this.

“By contrast, meteorological conditions and regional transport are governed by multiple scales of motion which result in distinct meteorological impacts on ambient pollutant levels (Levy et al., 2010, Dutton, 1976).”

L76: *“it can play”*

Response: We have rewritten the sentence, now it reads:

“Surface albedo and surface roughness are affected by the complex topography of river-valley regions, and those physical factors can affect circulation and cause changes in pollutant mass concentrations (Wei et al., 2020).”

L78: *“to converge”*

Response: We have corrected this. Then sentence now reads:

“Instead of being dispersed, they can be carried by the airflows over the mountains to converge at the bottom of the valley and increase the pollutants along the river (Zhao et al., 2015).”

L80: *“fascinated”*. Maybe too strong a word? May I suggest *“keen on studying”* instead. *“eBCs”* not defined.

Response: We changed the expression:

“Thus, we focused our study on the impacts of different scales of motion on source-specific equivalent BCs (eBCs), and we evaluated radiative effects of eBCs over a river-valley city.”

L92-93: *“located at the furthest west”*

Response: We corrected this mistake:

“Baoji is a typical river-valley city, located at the furthest west of the Guanzhong Plain, at an altitude from 450 to 800 m a.s.l. (Figure S1), Baoji has a complex topography and often suffering from severe pollution in winter.”

L93: replace *“suffers”* by *“suffering from”*

Response: Correction has made, see in the above response.

L107: *“Aurora”*

Response: We corrected the spelling.

L151: *“deconvolved”* rather than *“separated”*

Response: We have replace *“separated”* with *“deconvolved”*.

“The quantities of eBC generated from biomass burning versus fossil fuel combustion were deconvolved by an aethalometer model which uses Beer-Lambert’s Law to write the absorption coefficients equations, wavelengths and absorption Ångström exponents (AAEs) for the two different BC emission sources (Sandradewi et. al., 2008).”

L171: *“different scales”*

Response: Correction has been made:

“2.5 Indicators for the different scales of motion”

L230: *“minus”*

Response: We corrected the spelling:

“where DRE_{eBC} is the DRE of source-specific eBC, $F\downarrow$ and $F\uparrow$ are the downward and upward flux, $DRE_{eBC,ATM}$ is the DRE of the source-specific eBC for the atmospheric column, that is, the DRE at the top of the atmosphere ($DRE_{eBC,TOA}$) minus that at the surface ($DRE_{eBC,SUF}$).”

L235: *“was run”*

Response: We corrected this:

“For every solution, PMF was run 20 times. The $Q_{\text{true}}/Q_{\text{exp}}$ ratios from the 2- to 7-factor solutions were examined, and the values of a 4-factor solution were found most stable compared with others because the $Q_{\text{true}}/Q_{\text{exp}}$ values did not drop appreciably after the addition of one more factor (Figure S5).”

L236: “2-factor solution (...) 7-factor solution (...) 4-factor solution” + L237, L239

Response: We corrected this.

L279: “were calculated”

Response: Correction has been made:

“Thus, the AAE_{fossil} (1.26) and $MAC(880)_{\text{fossil}}$ ($7.1 \text{ m}^2 \text{ g}^{-1}$) were calculated as the mass-weighted averages (relative to the total EC) of AAE_{coal} ($MAC(880)_{\text{coal}}$) and AAE_{diesel} ($MAC(880)_{\text{diesel}}$) (Table S4)”

L282-283: “Their diurnal variations showed varied”. Please consider revising.

Response: We have rewritten this sentence. Now it reads:

“The results showed that eBC_{fossil} and eBC_{biomass} were only weakly correlated ($r = 0.3$, Figure S9), indicating a reasonably good separation, and furthermore, their diel variations showed different patterns (Figure 2).”

L282, 284: “diel” instead of “diurnal”

Response: We have changed the words. The sentences now read:

“The diel variations of eBC_{fossil} (Figure 2a) showed a bimodal pattern with two peaks at 9 a.m. and 7 p.m. local time, which are typical peak commuting hours, indicating that there were strong influences from traffic emissions.” And the response above.

L293: “New para here” should be deleted.

Response: We deleted it:

“Later the PBLH decreased rapidly, resulting in conditions unfavorable for dispersion, and then eBC_{fossil} rose quickly to the second peak at 7 p.m. After passing the evening peak in traffic, the eBC_{fossil} decreased dramatically.”

L331: rather “clean” instead of “clear”.

Response: This correction has been made:

“When the regional scale of motion became stronger (i.e., LWRS and RD), the average mass concentration of eBC_{fossil} ($2.15 \pm 1.62 \mu\text{g m}^{-3}$ and $1.69 \pm 1.36 \mu\text{g m}^{-3}$) and eBC_{biomass} ($0.86 \pm 1.58 \mu\text{g m}^{-3}$ and $0.93 \pm 0.72 \mu\text{g m}^{-3}$) were lower, presumably because strong winds cause the pollutants to mix with cleaner air.”

L333: “were carried”

Response: We corrected this:

“Interestingly, 19% of the total 75th to 100th percentile eBC_{biomass} was found under RD, and 55% of that was when ventilation good ($S_{bj} \geq 250\text{km}$, $R_{bj} \leq 0.2$, Figure 3, shaded grey). These findings imply that the high mass concentrations of eBC_{biomass} were carried by regional-scale airflow to the site.”

L360-362: Consider revising this sentence: “emissions at in” (delete “at”); “(~75%) of the total population of Baoji” can be replaced by “(that is to say 75%)”; “distributed located”, pick only one.

Response: We have rewritten the sentence, now it reads:

“This could be attributed to more intensive emissions in the eastern parts of Baoji because 75% of the total population of Baoji is located in this area (http://tjj.baoji.gov.cn/art/2020/10/15/art_9233_1216737.html, accessed on 25 September 2021, in Chinese).”

L432: “outweighed the regional-scale motion”

Response: Correction has been made:

“This illustrates that the BC pollution was more severe under the influences of local-scale motion outweighed regional-scale motions.”

L436: “found to be raised”

Response: We have corrected this sentence, now it reads:

“eBC_{fossil} most likely accumulated under the influence of strong local-scale motions, but eBC_{biomass} also was found to be increased with the enhanced regional scale of motions when the air masses from the southwest; this indicates that there were impacts from regional transport.”

L717: Figure 1 | x-axis title: “Pabs” instead of “babs”

Response: We thank review for pointing this out. We corrected this:

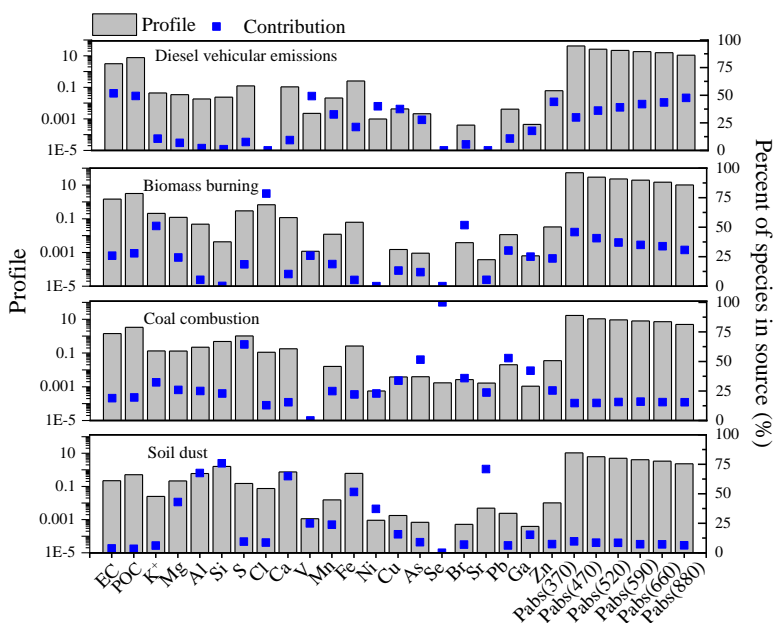


Figure R6. Four factors identified by source apportionment. Concentration ($\mu\text{g m}^{-3}$) of the chemical species and primary absorption coefficients (p_{abs}) (λ) at six wavelengths ($\lambda = 370, 470, 520, 590, 660, \text{ or } 880\text{nm}$) (M m^{-1}) for each source are shown in grey. The blue square represents the contribution of each chemical species to the four different factors.

L721: “diurnal” should be replaced by “diel” (24-hour period). At the least, standard deviations could be added for each hourly-averaged point; otherwise each point could be replaced by a box and whiskers that better show the dispersion of the raw data.

Response: The standard deviations have been added for the each point of Figure 2. Now it looks like this:

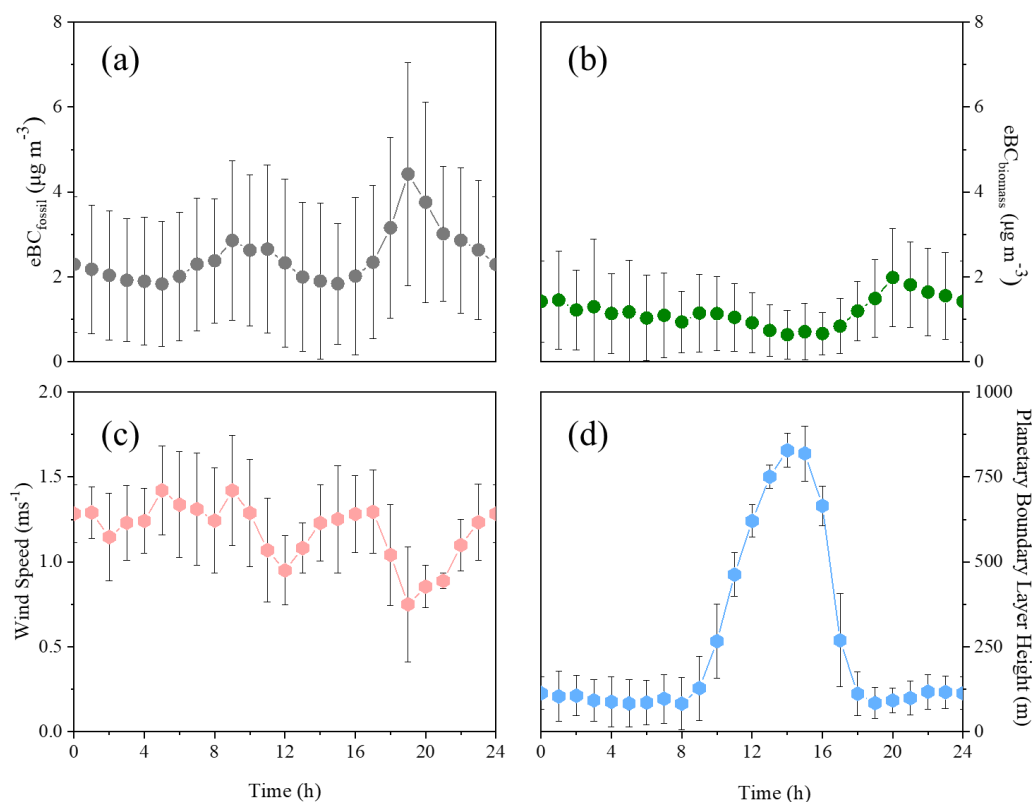


Figure R7. (a) Diel variations of the eBC from fossil fuel combustion ($\text{eBC}_{\text{fossil}}$) and (b) the eBC from biomass burning ($\text{eBC}_{\text{biomass}}$), (c) wind speed (m s^{-1}) and (d) planetary boundary layer height (m). The black bars of each hourly-averaged point show the standard deviation.

L724: Figure 3 caption should explain what the different marker colors and the shaded areas represent.

Response: We have revised the figure caption as follows:

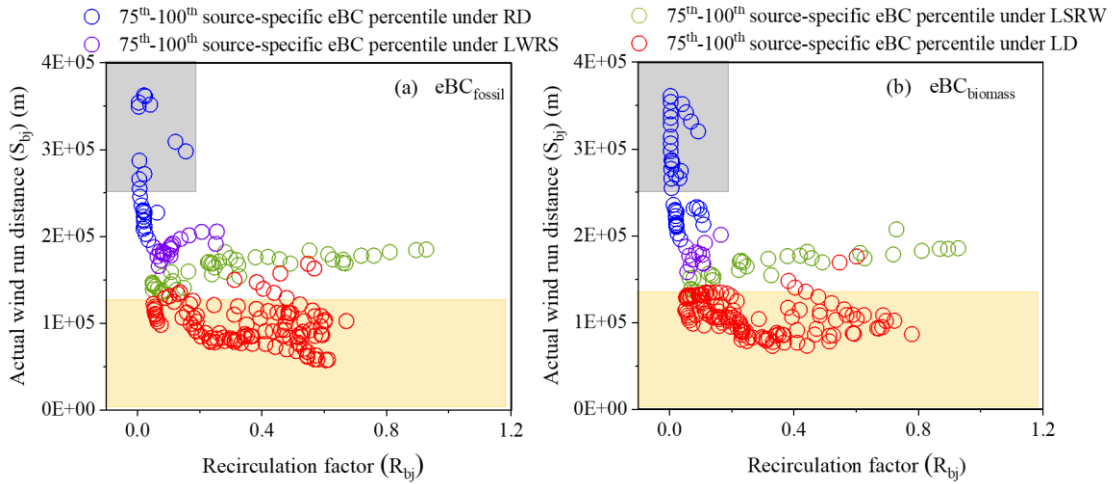


Figure R8. (a) The 75th – 100th percentile mass concentrations of the eBC from fossil fuel combustion (eBC_{fossil}) and (b) the eBC from biomass burning (eBC_{biomass}) under local scale dominance (LD, red circle), local scale strong and regional scale weak (LSRW, green circle), local scale weak regional scale strong (LWRS, purple circle) and regional scale dominance (RD, blue circle). S_{bj} is actual wind run distance at 100m height, R_{bj} is the recirculation factor, the grey area indicates good ventilation ($S_{bj} \geq 250\text{km}$, $R_{bj} \leq 0.2$), the yellow area indicates air stagnation ($S_{bj} \leq 130\text{km}$).

L731: Figure 5a | The 4th box and whisker plot (blue) should be labelled “fossil” and not “biomass” on the x-axis.

Response: We have re-drawn this figure and corrected the label as follows:

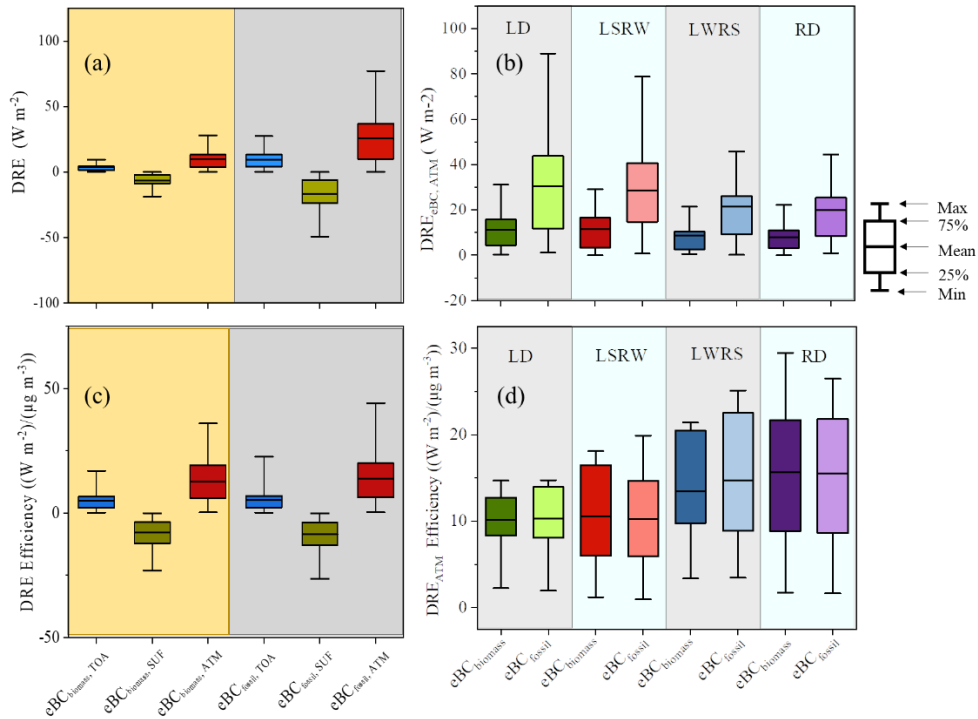


Figure R9. Direct radiative effect (DRE) of the eBC from fossil fuel combustion (eBC_{fossil}) shaded in grey and the eBC from biomass burning (eBC_{biomass}) shaded in yellow (a) in the top atmosphere (TOA), surface (SUF), and the atmosphere atmospheric column (ATM) and (b) the $DRE_{eBC,ATM}$ of two types of eBC under local scale dominance (LD) shaded in light grey labeled as LD, local scale strong and regional scale weak (LSRW) shaded in light blue labeled as LSRW, local scale weak regional scale strong (LWRS) shaded in light grey labeled with LWRS and regional scale dominance (RD) shaded in light blue labelled as RD (c) DRE efficiencies of eBC_{biomass} (shaded in yellow) and eBC_{fossil} (shaded by grey) in TOA, SUF and ATM (d) DRE efficiencies of eBC_{biomass} and eBC_{fossil} at ATM under LD (shaded in light grey labeled as LD), LSRW (shaded in light blue labeled as LSRW), LWRS (shaded in light grey labeled as LWRS) and RD (shaded in light blue labeled with RD).

Supplementary Information

Table S2 would look better if numbers were aligned with column titles.

Response: Thanks for the suggestion, we have aligned the number with column titles.

Table R7. Mass absorption cross sections (MAC) and absorption Ångström exponents (AAE) derived from the positive matrix factorization model

	Diesel vehicular missions	Coal combustion	Biomass burning	Fossil fuel combustion
MAC ($\text{m}^2 \text{g}^{-1}$)	6.7	7.5	9.5	7.1
AAE	1.07	1.74	2.13	1.26

Figure S1: Add a scale on both maps. Topography should be indicated on the closer range map.

Response: We have updated the map of the region in the supplementary materials. It can be seen in the response above.

Figure S2 caption: "the modelled $b_{\text{abs}}(500 \text{ nm})$ (respectively, SSA) and the observed $b_{\text{abs}}(520 \text{ nm})$ (resp. SSA)". Right now, it reads like a ratio of the two parameters.

Response: We thank reviewer's suggestion and have rewritten the caption as follows:

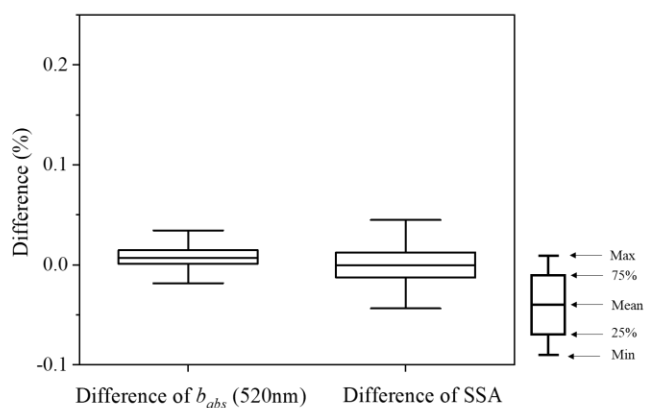


Figure R10. The difference between the modeled $b_{abs}(500\text{nm})$ (respectively, SSA) and the observed $b_{abs}(520\text{nm})$ (respectively, SSA).

Figures S4, S5 and S6: What does each point represent? (daily average, other?)

Response: The $b_{abs}(\lambda)$ in Figure S4 are daily averaged data. NO_x and EC in Figure S5 are daily averaged data. The $\text{eBC}_{\text{biomass}}$ and $\text{eBC}_{\text{fossil}}$ are hourly averaged data. We have added this into the caption for each figure as follows:

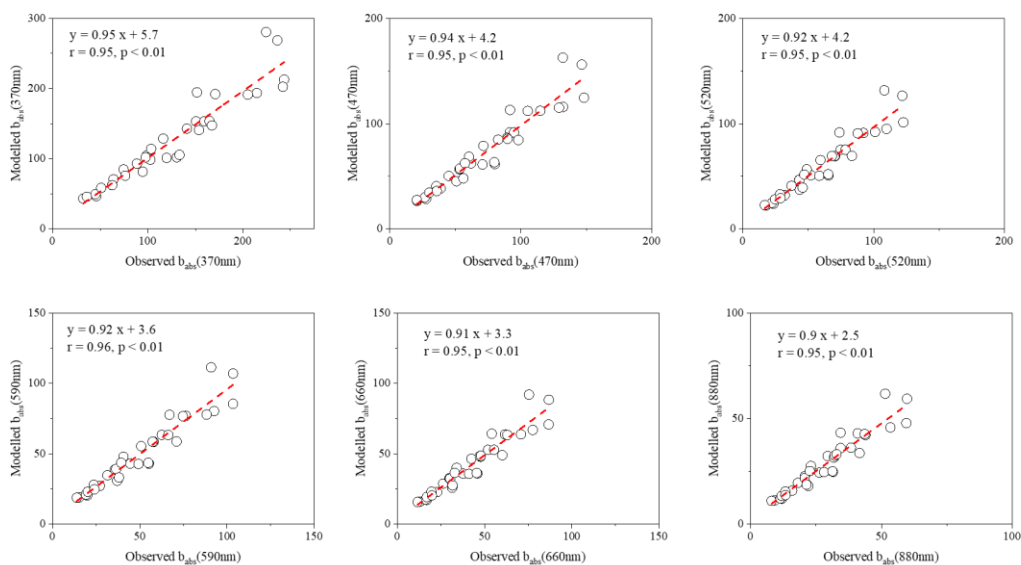


Figure R11. Relationship between the observed daily averaged $b_{abs}(\lambda)$ and positive matrix factorization modeled $b_{abs}(\lambda)$. λ includes 370, 470, 520, 590, 660 and 880nm. The red line is a linear fit.

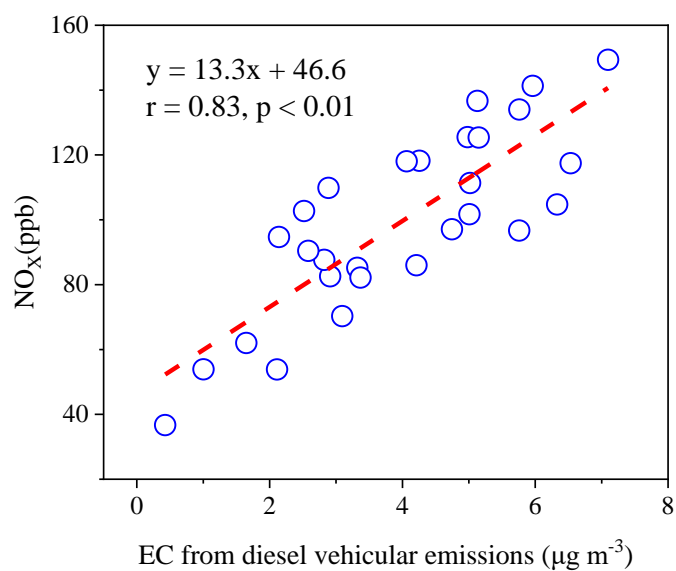


Figure R12. Linear regression of the daily averaged NO_x versus the daily averaged elemental carbon (EC) emitted from diesel vehicular emissions. The red line is the linear fit.

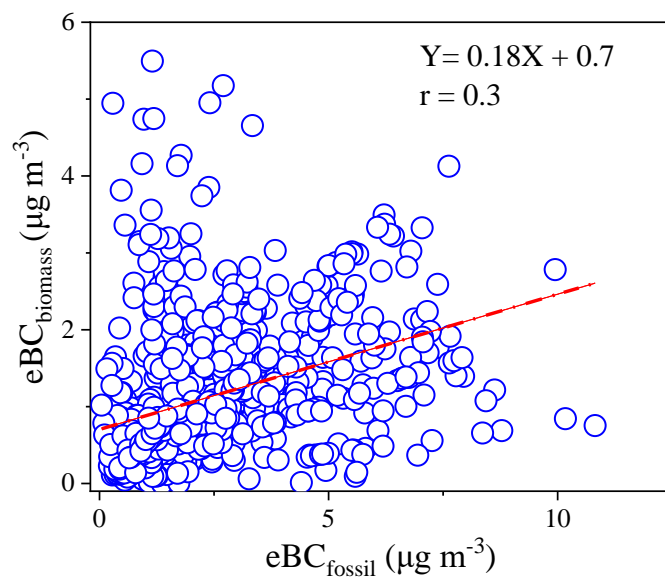


Figure R13. Relationship between hourly averaged eBC from biomass burning (eBC_{biomass}) and the eBC emitted from fossil fuel combustion (eBC_{fossil}). The red line is a linear fit.

Figure S9: “diurnal” should be replaced by “diel” (24-hour period). At the least, standard deviations could be added for each hourly-averaged point; otherwise each point could be replaced by a box and whisker that better shows the dispersion of the raw data.

Response: We have revised this figure with standard deviations:

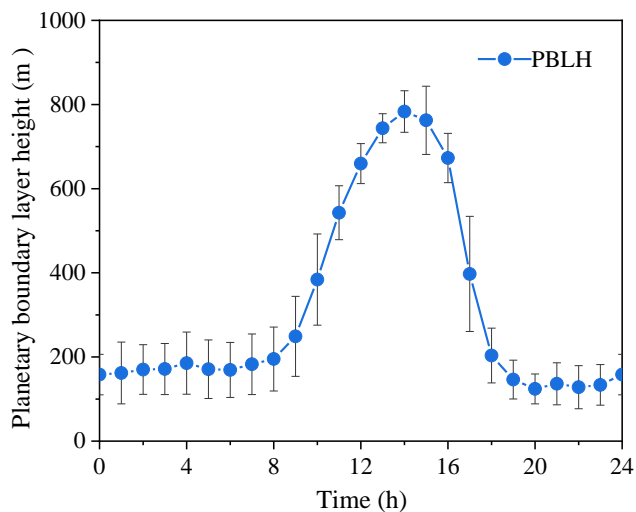


Figure R14. Diel variations of planetary boundary layer height (PBLH, m) under the dominance of regional scale of motion (RD), the blue dots represent the hourly-averaged PBLH and the black lines represent the standard deviations for each point.